

Can tensor-scalar induced GWs dominate PTA observations ?

Di Wu¹,^a Jing-Zhi Zhou¹,^{b,1} Yu-Ting Kuang¹,^{c,d} Zhi-Chao Li¹,^b
Zhe Chang¹,^{c,d} Qing-Guo Huang¹,^{a,d,e,1}

^aSchool of Fundamental Physics and Mathematical Sciences, Hangzhou Institute for Advanced Study, UCAS, Hangzhou 310024, China

^bCenter for Joint Quantum Studies and Department of Physics, School of Science, Tianjin University, Tianjin 300350, China

^cInstitute of High Energy Physics, Chinese Academy of Sciences, Beijing 100049, China

^dUniversity of Chinese Academy of Sciences, Beijing 100049, China

^eCAS Key Laboratory of Theoretical Physics, Institute of Theoretical Physics, Chinese Academy of Sciences

E-mail: wudi@ucas.ac.cn, zhoujingzhi@tju.edu.cn, kuangyt@ihep.ac.cn,
lizc@tju.edu.cn, changz@ihep.ac.cn, huangqg@itp.ac.cn

Abstract. Observational constraints on small-scale primordial gravitational waves are considerably weaker than those on large scales. We focus on scenarios with significant primordial gravitational waves and curvature perturbations on small scales, studying the energy density spectrum of the second-order tensor-scalar induced gravitational waves (TSIGWs). By leveraging current data from cosmic microwave background (CMB), baryon acoustic oscillations (BAO), and pulsar timing array (PTA), combined with the signal-to-noise ratio (SNR) analysis of Laser Interferometer Space Antenna (LISA), we can investigate how tensor-scalar induced gravitational waves affect observations on various scales, thus constraining the parameter space for primordial gravitational waves and curvature perturbations. The Bayes factor analysis suggests that tensor-scalar induced gravitational waves (TSIGWs)+primordial gravitational waves (PGWs) might be more likely to dominate current pulsar timing array (PTA) observations compared to supermassive black hole binary (SMBHB).

¹Corresponding author.

Contents

1	Introduction	1
2	Equations of motion of TSIGWs	2
3	Energy density spectra of TSIGWs	5
4	Detection of TSIGWs	7
4.1	PTA observations	8
4.2	Signal-to-noise ratio of LISA	9
4.3	Constraints from CMB and BAO	11
5	Conclusion and discussion	13

1 Introduction

Current cosmological observations indicate our universe is homogeneous and isotropic on large scales, as described by the Friedmann-Lemaître-Robertson-Walker (FLRW) metric [1]. Deviations from isotropy and homogeneity are described by cosmological perturbations in the FLRW spacetime, and according to its symmetries, these perturbations are decomposed into scalar, vector, and tensor perturbations [2, 3]. These types of cosmological perturbations play essential roles in cosmic evolution. Perturbations generated during inflation are known as primordial perturbations [4]. As the initial conditions for the subsequent evolution of the universe, primordial perturbations influence all later cosmological processes.

The cosmological observations allow us to constrain these primordial perturbations on different scales. As vector perturbations decay with $1/a^2$, we consider primarily primordial curvature (scalar) and primordial tensor perturbations (primordial gravitational waves) [5]. On large scales ($\gtrsim 1$ Mpc), the amplitude of primordial curvature perturbations A_ζ is tightly constrained by cosmic microwave background (CMB) and large-scale structure (LSS) observations to around $A_\zeta \sim 2 \times 10^{-9}$ [6–8]. The tensor-to-scalar ratio $r = A_h/A_\zeta$ is currently constrained below 0.06 [9–12]. However, on smaller scales ($\lesssim 1$ Mpc), constraints on primordial curvature and tensor perturbations are much weaker [13, 14]. Current cosmological observations allow for large primordial curvature perturbations and primordial gravitational waves (PGWs) on small scales. Large-amplitude primordial perturbations on small scales can generate significant observational effects after re-entering the horizon following inflation, leading to higher-order induced gravitational waves (GWs). If we neglect PGWs on small scales and only consider large-amplitude primordial curvature perturbations, the resulting higher-order GWs are known as scalar induced gravitational waves (SIGWs) [15–32]. When large primordial curvature perturbations and PGWs are both considered, the higher-order GWs induced by both are referred to as tensor-scalar induced gravitational waves (TSIGWs) [33–37]. Since the TSIGW is sourced by primordial perturbations with large amplitude on small scales ($\lesssim 1$ Mpc), it can be used as a probe to detect small-scale primordial power spectra [38].

In June 2023, the pulsar timing array (PTA) collaborations NANOGrav [39, 40], EPTA [41], Parkes PTA [42], and China PTA [43] reported evidence for an isotropic, stochastic background of GWs within the nHz frequency range. There are many potential sources for the stochastic gravitational wave backgrounds (SGWBs). For standard astrophysical sources, the PTA signal is predominantly attributed to supermassive black hole binaries (SMBHBs) [44, 45]. In addition, the PTA observations might also have a cosmological origin, such as first-order phase transitions [46–51], cosmic strings [52–56], and SIGWs [57–67]. In this paper, we consider the scenario where second-order TSIGWs dominate current SGWBs observations. It requires the

large primordial tensor perturbations on small scales ($\lesssim 1$ Mpc) which can be realized by various early-universe models, such as G^2 -inflation [68], sound speed resonance [69], and spectator fields [70]. In this case, the second-order GWs are induced by scalar-scalar, scalar-tensor, and tensor-tensor coupling source terms. The current PTA observations can be used as a probe to constrict the parameter space of small-scale primordial curvature and tensor power spectra. Furthermore, TSIGWs and PGWs can contribute as an extra radiation component, impacting the large-scale cosmological observations [71–73]. By combining current PTA observations on small scales with CMB and baryon acoustic oscillations (BAO) observational data, we can investigate second-order TSIGWs and constrain the parameter space of small-scale PGWs and curvature perturbations. In addition, since the influence of PGWs on the second-order TSIGWs is primarily concentrated in the high-frequency region, we can rigorously analyze the signal-to-noise ratio (SNR) of Laser Interferometer Space Antenna (LISA) based on theoretical results of TSIGWs, thus quantitatively describing the impact of PGWs on the total energy density spectrum of GWs in the high-frequency region.

This paper is organized as follows. In Sec. 2, we review the basic calculations of TSIGWs. In Sec. 3, we study the current total energy density spectra of GWs. The explicit expressions of the power spectra of TSIGWs are given in this section. In Sec. 4, we investigate the constraints on the parameter space of TSIGWs and the primordial power spectrum through combined experimental observations from CMB, BAO, PTA, and LISA. Finally, we summarize our results and give some discussions in Sec. 5.

2 Equations of motion of TSIGWs

In this section, we briefly review the equations of motion of second-order TSIGWs [33–36]. The line element of perturbed spacetime in Newtonian gauge is expressed as [2]

$$ds^2 = a^2 \left[- \left(1 + 2\phi^{(1)} \right) d\eta^2 + \left(\left(1 - 2\psi^{(1)} \right) \delta_{ij} + h_{ij}^{(1)} + \frac{1}{2} h_{ij}^{(2)} \right) dx^i dx^j \right], \quad (2.1)$$

where $\phi^{(1)}$ and $\psi^{(1)}$ are first-order scalar perturbations, $h_{ij}^{(n)}$ ($n = 1, 2$) are n -order tensor perturbations. In the study of second-order TSIGWs, we need to consider large-amplitude PGWs on small scales. Therefore, unlike the usual second-order SIGWs, we retain the first-order tensor perturbation $h_{ij}^{(1)}$ in the metric perturbation given in Eq. (2.1). By substituting the metric perturbation in Eq. (2.1) into the Einstein field equations, we can obtain the equations of motion for the second-order TSIGWs [33]

$$h_{ij}^{(2)''}(\eta, \mathbf{x}) + 2\mathcal{H}h_{ij}^{(2)'}(\eta, \mathbf{x}) - \Delta h_{ij}^{(2)}(\eta, \mathbf{x}) = -4\Lambda_{ij}^{lm} \left(\mathcal{S}_{lm,\phi\phi}^{(2)} + \mathcal{S}_{lm,\phi h}^{(2)} + \mathcal{S}_{lm,hh}^{(2)} \right), \quad (2.2)$$

where $\mathcal{H} = a'/a$ is the conformal Hubble parameter, and Λ_{ij}^{lm} is the decomposed operator to extract the transverse and traceless terms [26]. In this paper, we consider the second-order TSIGWs during the radiation-dominated (RD) era, where $\mathcal{H} = 1/\eta$ and $w = c_s^2 = 1/3$. The three types of source terms in Eq. (2.2) can be expressed as

$$\begin{aligned} \mathcal{S}_{lm,\phi\phi}^{(2)}(\eta, \mathbf{x}) &= \partial_l \phi^{(1)} \partial_m \phi^{(1)} + 4\phi^{(1)} \partial_l \partial_m \phi^{(1)} - \frac{1}{\mathcal{H}} \left(\partial_l \phi^{(1)'} \partial_m \phi^{(1)} + \partial_l \phi^{(1)} \partial_m \phi^{(1)'} \right) \\ &\quad - \frac{1}{\mathcal{H}^2} \partial_l \phi^{(1)'} \partial_m \phi^{(1)'} , \end{aligned} \quad (2.3)$$

$$\mathcal{S}_{lm,\phi h}^{(2)}(\eta, \mathbf{x}) = 10\mathcal{H}h_{lm}^{(1)}\phi^{(1)'} + 3h_{lm}^{(1)}\phi^{(1)''} - \frac{5}{3}h_{lm}^{(1)}\Delta\phi^{(1)} - 2\partial_b h_{lm}^{(1)}\partial^b \phi^{(1)} - 2\phi^{(1)}\Delta h_{lm}^{(1)}, \quad (2.4)$$

$$\begin{aligned} \mathcal{S}_{lm,hh}^{(2)}(\eta, \mathbf{x}) &= \frac{1}{2} \left(-h_l^{b,(1)'} h_{mb}^{(1)'} + \partial_c h_{mb}^{(1)} \partial^c h_l^{b,(1)} - h^{bc,(1)} \partial_c \partial_m h_{lb}^{(1)} - \partial_b h_{mc}^{(1)} \partial^c h_l^{b,(1)} \right. \\ &\quad \left. + \frac{1}{2} h^{bc,(1)} \partial_l \partial_m h_{bc}^{(1)} + h^{bc,(1)} \partial_c \partial_b h_{lm}^{(1)} - h^{bc,(1)} \partial_c \partial_l h_{mb}^{(1)} \right). \end{aligned} \quad (2.5)$$

As shown in Eq. (2.3)–Eq. (2.5), the source term $S_{lm,\phi\phi}$ is identical to the source term of the second-order SIGWs [15, 74]. The source term $S_{lm,\phi h}$ is composed of the product of the first-order scalar perturbation $\phi^{(1)}$ and the first-order tensor perturbation $h_{lm}^{(1)}$. The source terms $S_{lm,hh}$ are composed of the first-order tensor perturbation $h_{lm}^{(1)}$. In momentum space, the solutions of first-order scalar and tensor perturbations are

$$\psi(\eta, \mathbf{k}) = \phi(\eta, \mathbf{k}) = \frac{2}{3}\zeta_{\mathbf{k}}T_{\phi}(|\mathbf{k}|\eta) , \quad h^{\lambda,(1)}(\eta, \mathbf{k}) = \mathbf{h}_{\mathbf{k}}^{\lambda}T_h(|\mathbf{k}|\eta) , \quad (2.6)$$

where $\zeta_{\mathbf{k}}$ and $\mathbf{h}_{\mathbf{k}}^{\lambda}$ are the primordial curvature and tensor perturbations, respectively. During the RD era, the transfer functions $T_{\phi}(|\mathbf{k}|\eta)$ and $T_h(|\mathbf{k}|\eta)$ in Eq. (2.6) are given by [74]

$$T_{\phi}(x) = \frac{9}{x^2} \left(\frac{\sqrt{3}}{x} \sin\left(\frac{x}{\sqrt{3}}\right) - \cos\left(\frac{x}{\sqrt{3}}\right) \right) , \quad T_h(x) = \frac{\sin x}{x} , \quad (2.7)$$

where we have set $x \equiv |\mathbf{k}|\eta$. By substituting the analytical expressions of first-order perturbations in Eq. (2.6) and Eq. (2.7) into Eq. (2.3)–Eq. (2.5), we can derive the specific expressions for the three types of source terms of second-order TSIGWs. Using the Green's function approach to solve Eq. (2.2), we obtain the expression for second-order TSIGWs as

$$h^{\lambda,(2)}(\eta, \mathbf{k}) = \sum_{i=1}^7 h_i^{\lambda,(2)}(\eta, \mathbf{k}) , \quad (2.8)$$

where $h^{\lambda,(2)}(\eta, \mathbf{k}) = \varepsilon^{\lambda,ij}(\mathbf{k})h_{ij}^{(2)}(\eta, \mathbf{k})$ and $S^{\lambda,(2)}(\eta, \mathbf{k}) = -\varepsilon^{\lambda,lm}(\mathbf{k})S_{lm}^{(2)}(\eta, \mathbf{k})$. And the $\varepsilon_{ij}^{\lambda}(\mathbf{k})$ is polarization tensor. The explicit expressions of $h_i^{\lambda,(2)}(\eta, \mathbf{k})$ ($i = 1 \sim 7$) in Eq. (2.8) are given by

$$h_1^{\lambda,(2)}(\eta, \mathbf{k}) = -\frac{4}{9} \int \frac{d^3p}{(2\pi)^{3/2}} \varepsilon^{\lambda,lm}(\mathbf{k}) p_l p_m I_1^{(2)}(u, v, x) \zeta_{\mathbf{k}-\mathbf{p}} \zeta_{\mathbf{p}} , \quad (2.9)$$

$$h_2^{\lambda,(2)}(\eta, \mathbf{k}) = -\frac{2}{3} \int \frac{d^3p}{(2\pi)^{3/2}} \varepsilon^{\lambda,lm}(\mathbf{k}) \varepsilon_{lm}^{\lambda_1}(\mathbf{p}) k^2 I_2^{(2)}(u, v, x) \zeta_{\mathbf{k}-\mathbf{p}} \mathbf{h}_{\mathbf{p}}^{\lambda_1} , \quad (2.10)$$

$$h_3^{\lambda,(2)}(\eta, \mathbf{k}) = - \int \frac{d^3p}{(2\pi)^{3/2}} \varepsilon^{\lambda,lm}(\mathbf{k}) \varepsilon_l^{\lambda_1,b}(\mathbf{k}-\mathbf{p}) \varepsilon_{bm}^{\lambda_2}(\mathbf{p}) k^2 I_3^{(2)}(u, v, x) \mathbf{h}_{\mathbf{k}-\mathbf{p}}^{\lambda_1} \mathbf{h}_{\mathbf{p}}^{\lambda_2} , \quad (2.11)$$

$$h_4^{\lambda,(2)}(\eta, \mathbf{k}) = - \int \frac{d^3p}{(2\pi)^{3/2}} \varepsilon^{\lambda,lm}(\mathbf{k}) \varepsilon^{\lambda_1,bc}(\mathbf{k}-\mathbf{p}) \left(2\varepsilon_{mb}^{\lambda_2}(\mathbf{p}) p_c p_l \right) \\ \times I_4^{(2)}(u, v, x) \mathbf{h}_{\mathbf{k}-\mathbf{p}}^{\lambda_1} \mathbf{h}_{\mathbf{p}}^{\lambda_2} , \quad (2.12)$$

$$h_5^{\lambda,(2)}(\eta, \mathbf{k}) = - \int \frac{d^3p}{(2\pi)^{3/2}} \varepsilon^{\lambda,lm}(\mathbf{k}) \varepsilon_{mc}^{\lambda_1}(\mathbf{k}-\mathbf{p}) \varepsilon_{lb}^{\lambda_2}(\mathbf{p}) (k-p)^b p^c \\ \times I_5^{(2)}(u, v, x) \mathbf{h}_{\mathbf{k}-\mathbf{p}}^{\lambda_1} \mathbf{h}_{\mathbf{p}}^{\lambda_2} , \quad (2.13)$$

$$h_6^{\lambda,(2)}(\eta, \mathbf{k}) = \int \frac{d^3p}{(2\pi)^{3/2}} \varepsilon^{\lambda,lm}(\mathbf{k}) \varepsilon_{bc}^{\lambda_1}(\mathbf{k}-\mathbf{p}) \varepsilon_{lm}^{\lambda_2}(\mathbf{p}) p^b p^c I_6^{(2)}(u, v, x) \mathbf{h}_{\mathbf{k}-\mathbf{p}}^{\lambda_1} \mathbf{h}_{\mathbf{p}}^{\lambda_2} , \quad (2.14)$$

$$h_7^{\lambda,(2)}(\eta, \mathbf{k}) = \int \frac{d^3p}{(2\pi)^{3/2}} \varepsilon^{\lambda,lm}(\mathbf{k}) \varepsilon^{\lambda_1,bc}(\mathbf{k}-\mathbf{p}) \varepsilon_{bc}^{\lambda_2}(\mathbf{p}) \frac{p_l p_m}{2} I_7^{(2)}(u, v, x) \mathbf{h}_{\mathbf{k}-\mathbf{p}}^{\lambda_1} \mathbf{h}_{\mathbf{p}}^{\lambda_2} . \quad (2.15)$$

Here, based on the specific form of the source term, we decompose the contributions of the source term $S_{lm,hh}^{(2)}$ into five parts: $h_3^{\lambda,(2)} \sim h_7^{\lambda,(2)}$. We defined $|\mathbf{k}-\mathbf{p}| = u|\mathbf{k}|$ and $|\mathbf{p}| = v|\mathbf{k}|$. The kernel functions $I_i^{(2)}(u, v, x)$ in Eq. (2.9)–Eq. (2.15) are given by

$$I_i^{(2)}(u, v, x) = \frac{4}{k^2} \int_0^x d\bar{x} \left(\frac{\bar{x}}{x} \sin(x-\bar{x}) f_i(u, v, \bar{x}) \right) , \quad (i = 1 \sim 7) , \quad (2.16)$$

where

$$f_1^{(2)}(u, v, x) = x^2 uv \frac{d}{d(ux)} T_\phi(ux) \frac{d}{d(vx)} T_\phi(vx) + 2ux T_\phi(vx) \frac{d}{d(ux)} T_\phi(ux) + 3T_\phi(ux) T_\phi(vx), \quad (2.17)$$

$$f_2^{(2)}(u, v, x) = \frac{10u}{x} T_h(vx) \frac{d}{d(ux)} T_\phi(ux) + 3u^2 T_h(vx) \frac{d^2}{d(ux)^2} T_\phi(ux) + \frac{5}{3} u^2 T_\phi(ux) T_h(vx) + (1 - v^2 - u^2) T_\phi(ux) T_h(vx) + 2v^2 T_\phi(ux) T_h(vx), \quad (2.18)$$

$$f_3^{(2)}(u, v, x) = -\frac{1 - u^2 - v^2}{4} T_h(ux) T_h(vx) - \frac{uv}{2} \frac{d}{d(ux)} T_h(ux) \frac{d}{d(vx)} T_h(vx), \quad (2.19)$$

$$f_i^{(2)}(u, v, x) = \frac{1}{2} T_h(ux) T_h(vx), \quad (i = 4, 5, 6, 7). \quad (2.20)$$

The analytic expressions of the second-order kernel functions $I_i^{(2)}(i = 1, 2, \dots, 7)$ in Eq. (2.16) are given by

$$k^2 I_1^{(2)}(u, v, x \rightarrow \infty) = \frac{27(u^2 + v^2 - 3)}{u^3 v^3 x} \left(\sin x (-4uv + (u^2 + v^2 - 3) \ln \left| \frac{3 - (u+v)^2}{3 - (u-v)^2} \right|) - \pi(u^2 + v^2 - 3) \Theta(v + u - \sqrt{3}) \cos x \right), \quad (2.21)$$

$$k^2 I_2^{(2)}(u, v, x \rightarrow \infty) = \frac{\sqrt{3}(u^2 - 3(1-v)^2)}{16u^3 vx} \left[\sin x \left((u^2 - 3(1+v)^2) \ln \left| \frac{(u - \sqrt{3}v)^2 - 3}{(u + \sqrt{3}v)^2 - 3} \right| - \frac{4uv(u^2 - 9v^2 + 9)}{\sqrt{3}(u^2 - 3(1-v)^2)} \right) - \pi(u^2 - 3(1+v)^2) \times \Theta(u + \sqrt{3}v - \sqrt{3}) \cos x \right], \quad (2.22)$$

$$k^2 I_3^{(2)}(u, v, x) = \frac{\sin x}{4x} - \frac{\sin(ux) \sin(vx)}{4uvx^2}, \quad (2.23)$$

$$k^2 I_i^{(2)}(u, v, x) = \frac{(x - \sin x) \sin(ux) \sin(vx)}{2uvx^3}, \quad (i = 4, 5, 6, 7), \quad (2.24)$$

where we have used the following approximations: $\lim_{x \rightarrow \pm\infty} \text{Si}(x) = \pm\pi/2$ and $\lim_{x \rightarrow \infty} \text{Ci}(x) = 0$ in Eq. (2.21) and Eq. (2.22). $\Theta(x)$ represents the Heaviside theta function. Eq. (2.23) and Eq. (2.24) provide the analytical expressions for the kernel functions corresponding to the first-order tensor source term. Similar to Eq. (2.21) and Eq. (2.22), when calculating the energy density spectrum of gravitational waves, we can use the oscillating average relations $\lim_{x \rightarrow \infty} \sin^2 x = 1/2$, $\lim_{x \rightarrow \infty} \cos^2 x = 1/2$, and $\lim_{x \rightarrow \infty} \cos x \sin x = 0$ to derive the approximate expression for the kernel function when $x \rightarrow \infty$ [75]. In this section, we derived the equations of motion of second-order TSIGWs using higher-order cosmological perturbation theory and solved them in momentum space. It is worth noting that we can also directly obtain the specific expressions for second-order TSIGWs in Eq. (2.9)–Eq. (2.15) using the vertex rules of higher-order cosmological perturbations, without deriving or solving the second-order cosmological perturbation equations. Detailed discussion can be found in Ref. [76]. Moreover, the specific expressions of the second-order kernel functions $I_i^{(2)}(u, v, x)$ given above apply to TSIGWs during the RD era. These results can be extended to the study of TSIGWs in other dominant eras, such as the early matter-dominated era [77–80].

3 Energy density spectra of TSIGWs

The total energy density fraction of GWs up to second order can be written as [81]

$$\begin{aligned}\Omega_{\text{GW}}^{\text{tot}}(\eta, k) &= \frac{\rho_{\text{GW}}^{(1)}(\eta, k) + \frac{1}{4}\rho_{\text{GW}}^{(2)}(\eta, k)}{\rho_{\text{tot}}(\eta)} \\ &= \frac{1}{6} \left(\frac{k}{a(\eta)H(\eta)} \right)^2 \left(\mathcal{P}_h^{(1)}(\eta, k) + \frac{1}{4}\mathcal{P}_h^{(2)}(\eta, k) \right),\end{aligned}\quad (3.1)$$

where

$$\mathcal{P}_h^{(1)}(\eta, k) = \mathcal{P}_h^{(1)}(k) (T_h(x))^2 \quad (3.2)$$

is the primordial power spectrum of first-order GWs $h_{ij}^{(1)}$. $\mathcal{P}_h^{(1)}(k)$ in Eq. (3.2) represents the power spectrum of PGWs. In Eq. (3.1), $\mathcal{P}_h^{(2)}(\eta, k)$ represents the power spectrum of second-order TSIGWs. The power spectra of n -th order GWs $\mathcal{P}_h^{(n)}(\mathbf{k}, \eta)$ in Eq. (3.1) are defined as

$$\langle h^{\lambda, (n)}(\mathbf{k}, \eta) h^{\lambda', (n)}(\mathbf{k}', \eta) \rangle = \delta^{\lambda\lambda'} \delta(\mathbf{k} + \mathbf{k}') \frac{2\pi^2}{k^3} \mathcal{P}_h^{(n)}(k, \eta). \quad (3.3)$$

As shown in Eq. (3.3), the power spectrum of GWs can be calculated in terms of the corresponding two-point function. By substituting Eq. (2.9)–Eq. (2.15) into Eq. (3.3), we obtain the explicit expression of the power spectra of second order TSIGWs [33]

$$\mathcal{P}_h^{(2)} = \mathcal{P}_h^{(2),11} + \mathcal{P}_h^{(2),22} + \sum_{i,j=3}^7 \mathcal{P}_h^{(2),ij}, \quad (3.4)$$

where

$$\begin{aligned}\mathcal{P}_h^{(2),11} &= \frac{1}{4} \int_0^\infty dv \int_{|1-v|}^{|1+v|} du \left(\frac{4v^2 - (1 + v^2 - u^2)^2}{4uv} \right)^2 \left(k^2 I_1^{(2)}(u, v, x) \right)^2 \\ &\quad \times \frac{4}{9} \mathcal{P}_\zeta^{(1)}(ku) \frac{4}{9} \mathcal{P}_\zeta^{(1)}(vk),\end{aligned}\quad (3.5)$$

$$\begin{aligned}\mathcal{P}_h^{(2),22} &= \frac{1}{4} \int_0^\infty dv \int_{|1-v|}^{|1+v|} du \frac{1}{64(uv)^2} \left(\frac{16(-u^2 + v^2 + 1)^2}{v^2} + \left(\frac{(-u^2 + v^2 + 1)^2}{v^2} + 4 \right)^2 \right) \\ &\quad \times \frac{4}{9} \left(k^2 I_2^{(2)}(u, v, x) \right)^2 \mathcal{P}_\zeta^{(1)}(ku) \mathcal{P}_h^{(1)}(vk),\end{aligned}\quad (3.6)$$

$$\begin{aligned}\mathcal{P}_h^{(2),ij} &= \frac{1}{4} \int_0^\infty dv \int_{|1-v|}^{|1+v|} du \frac{\mathbb{P}^{ij}(u, v)}{(uv)^2} \left(k^2 I_i^{(2)}(u, v, x) k^2 I_j^{(2)}(u, v, x) \right) \\ &\quad \times \mathcal{P}_h^{(1)}(ku) \mathcal{P}_h^{(1)}(vk), \quad (i, j = 3 \sim 7).\end{aligned}\quad (3.7)$$

In Eq. (3.5)–Eq. (3.7), $\mathcal{P}_h^{(2),11}$, $\mathcal{P}_h^{(2),22}$, and $\mathcal{P}_h^{(2),ij}$ represent the second-order power spectra from scalar-scalar, scalar-tensor, and tensor-tensor coupling source terms, respectively. These contributions depend on the amplitudes and shapes of the primordial power spectra $\mathcal{P}_\zeta^{(1)}(k)$ and $\mathcal{P}_h^{(1)}(k)$. As shown in Fig. 1, the power spectra of second-order TSIGWs correspond to the one-loop diagrams in higher-order cosmological perturbation theory [76]. More precisely, Fig. (1a) \sim Fig. (1c) correspond to the power spectrum of second-order SIGWs in Eq. (3.5), Fig. (1d) \sim Fig. (1f) correspond to the power spectrum of second-order GWs induced by primordial tensor

perturbations in Eq. (3.7), and Fig. (1g) corresponds to the power spectrum of second-order GWs induced by tensor-scalar source terms in Eq. (3.6). Since the integration over the azimuth angle of momentum \mathbf{p} is zero, Fig. (1c) and Fig. (1f) do not contribute to the power spectrum of TsigWs. The momentum polynomials $\mathbb{P}^{ij}(u, v)$ in Eq. (3.7) are given in Table. 1. In the calculation of the power spectra $\mathcal{P}_h^{(2),ij}$, we encounter the four-point correlation function of PGWs

$$\begin{aligned} \langle \mathbf{h}_{\mathbf{k}-\mathbf{p}}^{\lambda_1} \mathbf{h}_{\mathbf{p}}^{\lambda_2} \mathbf{h}_{\mathbf{k}'-\mathbf{p}'}^{\lambda_1'} \mathbf{h}_{\mathbf{p}'}^{\lambda_2'} \rangle &= \langle \mathbf{h}_{\mathbf{k}-\mathbf{p}}^{\lambda_1} \mathbf{h}_{\mathbf{k}'-\mathbf{p}'}^{\lambda_1'} \rangle \langle \mathbf{h}_{\mathbf{p}}^{\lambda_2} \mathbf{h}_{\mathbf{p}'}^{\lambda_2'} \rangle + \langle \mathbf{h}_{\mathbf{k}-\mathbf{p}}^{\lambda_1} \mathbf{h}_{\mathbf{p}'}^{\lambda_2'} \rangle \langle \mathbf{h}_{\mathbf{p}}^{\lambda_2} \mathbf{h}_{\mathbf{k}'-\mathbf{p}'}^{\lambda_1'} \rangle \\ &= \delta(\mathbf{k} + \mathbf{k}') \frac{(2\pi^2)^2}{p^3 |\mathbf{k} - \mathbf{p}|^3} \left(\delta^{\lambda_1 \lambda_1'} \delta^{\lambda_2 \lambda_2'} \delta(\mathbf{p} + \mathbf{p}') + \delta^{\lambda_1 \lambda_2'} \delta^{\lambda_2 \lambda_1'} \delta(\mathbf{k}' - \mathbf{p}' + \mathbf{p}) \right) \\ &\times \mathcal{P}_h(|\mathbf{k} - \mathbf{p}|) \mathcal{P}_h(|\mathbf{p}|). \end{aligned} \quad (3.8)$$

By integrating over the momentum \mathbf{p}' , we derive the substitution relation: $\mathbf{p}' \rightarrow -\mathbf{p}$ and $\mathbf{p}' \rightarrow \mathbf{p} - \mathbf{k}$. Then, we can express the momentum polynomial \mathbb{P}^{ij} in Table. 1 as a function of $u = |\mathbf{k} - \mathbf{p}|/|\mathbf{k}|$ and $v = |\mathbf{p}|/|\mathbf{k}|$.

$k^4 \mathbb{P}^{ij}$	$i = 3$
$j = 3$	$\delta^{\lambda\lambda'} \left(k^2 \varepsilon^{\lambda,lm}(\mathbf{k}) \varepsilon_l^{\lambda_1,b}(\mathbf{k}-\mathbf{p}) \varepsilon_{bm}^{\lambda_2}(\mathbf{p}) \right) \left(k'^2 \varepsilon^{\lambda',lm}(\mathbf{k}') \varepsilon_l^{\lambda_1',b}(\mathbf{k}'-\mathbf{p}') \varepsilon_{bm}^{\lambda_2'}(\mathbf{p}') \right)$
$j = 4$	$\delta^{\lambda\lambda'} \left(k^2 \varepsilon^{\lambda,lm}(\mathbf{k}) \varepsilon_l^{\lambda_1,b}(\mathbf{k}-\mathbf{p}) \varepsilon_{bm}^{\lambda_2}(\mathbf{p}) \right) \left(\varepsilon^{\lambda',lm}(\mathbf{k}') \varepsilon^{\lambda_1',bc}(\mathbf{k}'-\mathbf{p}') \left(2\varepsilon_{mb}^{\lambda_2'}(\mathbf{p}') p'_c p'_l \right) \right)$
$j = 5$	$\delta^{\lambda\lambda'} \left(k^2 \varepsilon^{\lambda,lm}(\mathbf{k}) \varepsilon_l^{\lambda_1,b}(\mathbf{k}-\mathbf{p}) \varepsilon_{bm}^{\lambda_2}(\mathbf{p}) \right) \left(\varepsilon^{\lambda',lm}(\mathbf{k}') \varepsilon_{mc}^{\lambda_1'}(\mathbf{k}'-\mathbf{p}') \varepsilon_{lb}^{\lambda_2'}(\mathbf{p}') (k'-p')^b p'^c \right)$
$j = 6$	$\delta^{\lambda\lambda'} \left(k^2 \varepsilon^{\lambda,lm}(\mathbf{k}) \varepsilon_l^{\lambda_1,b}(\mathbf{k}-\mathbf{p}) \varepsilon_{bm}^{\lambda_2}(\mathbf{p}) \right) \left(\varepsilon^{\lambda',lm}(\mathbf{k}') \varepsilon_{bc}^{\lambda_1'}(\mathbf{k}'-\mathbf{p}') \varepsilon_{lm}^{\lambda_2'}(\mathbf{p}') p'^b p'^c \right)$
$j = 7$	$\delta^{\lambda\lambda'} \left(k^2 \varepsilon^{\lambda,lm}(\mathbf{k}) \varepsilon_l^{\lambda_1,b}(\mathbf{k}-\mathbf{p}) \varepsilon_{bm}^{\lambda_2}(\mathbf{p}) \right) \left(\varepsilon^{\lambda',lm}(\mathbf{k}') \varepsilon^{\lambda_1',bc}(\mathbf{k}'-\mathbf{p}') \varepsilon_{bc}^{\lambda_2'}(\mathbf{p}') p'_l p'_m \right)$
$k^4 \mathbb{P}^{ij}$	$i = 4$
$j = 4$	$\delta^{\lambda\lambda'} \left(\varepsilon^{\lambda,lm}(\mathbf{k}) \varepsilon^{\lambda_1,bc}(\mathbf{k}-\mathbf{p}) \left(2\varepsilon_{mb}^{\lambda_2}(\mathbf{p}) p_c p_l \right) \right) \left(\varepsilon^{\lambda',lm}(\mathbf{k}') \varepsilon^{\lambda_1',bc}(\mathbf{k}'-\mathbf{p}') \left(2\varepsilon_{mb}^{\lambda_2'}(\mathbf{p}') p'_c p'_l \right) \right)$
$j = 5$	$\delta^{\lambda\lambda'} \left(\varepsilon^{\lambda,lm}(\mathbf{k}) \varepsilon^{\lambda_1,bc}(\mathbf{k}-\mathbf{p}) \left(2\varepsilon_{mb}^{\lambda_2}(\mathbf{p}) p_c p_l \right) \right) \left(\varepsilon^{\lambda',lm}(\mathbf{k}') \varepsilon_{mc}^{\lambda_1'}(\mathbf{k}'-\mathbf{p}') \varepsilon_{lb}^{\lambda_2'}(\mathbf{p}') (k'-p')^b p'^c \right)$
$j = 6$	$\delta^{\lambda\lambda'} \left(\varepsilon^{\lambda,lm}(\mathbf{k}) \varepsilon^{\lambda_1,bc}(\mathbf{k}-\mathbf{p}) \left(2\varepsilon_{mb}^{\lambda_2}(\mathbf{p}) p_c p_l \right) \right) \left(\varepsilon^{\lambda',lm}(\mathbf{k}') \varepsilon_{bc}^{\lambda_1'}(\mathbf{k}'-\mathbf{p}') \varepsilon_{lm}^{\lambda_2'}(\mathbf{p}') p'^b p'^c \right)$
$j = 7$	$\delta^{\lambda\lambda'} \left(\varepsilon^{\lambda,lm}(\mathbf{k}) \varepsilon^{\lambda_1,bc}(\mathbf{k}-\mathbf{p}) \left(2\varepsilon_{mb}^{\lambda_2}(\mathbf{p}) p_c p_l \right) \right) \left(\varepsilon^{\lambda',lm}(\mathbf{k}') \varepsilon^{\lambda_1',bc}(\mathbf{k}'-\mathbf{p}') \varepsilon_{bc}^{\lambda_2'}(\mathbf{p}') p'_l p'_m \right)$
$k^4 \mathbb{P}^{ij}$	$i = 5$
$j = 5$	$\delta^{\lambda\lambda'} \left(\varepsilon^{\lambda,lm}(\mathbf{k}) \varepsilon_{mc}^{\lambda_1}(\mathbf{k}-\mathbf{p}) \varepsilon_{lb}^{\lambda_2}(\mathbf{p}) (k-p)^b p^c \right) \left(\varepsilon^{\lambda',lm}(\mathbf{k}') \varepsilon_{mc}^{\lambda_1'}(\mathbf{k}'-\mathbf{p}') \varepsilon_{lb}^{\lambda_2'}(\mathbf{p}') (k'-p')^b p'^c \right)$
$j = 6$	$\delta^{\lambda\lambda'} \left(\varepsilon^{\lambda,lm}(\mathbf{k}) \varepsilon_{mc}^{\lambda_1}(\mathbf{k}-\mathbf{p}) \varepsilon_{lb}^{\lambda_2}(\mathbf{p}) (k-p)^b p^c \right) \left(\varepsilon^{\lambda',lm}(\mathbf{k}') \varepsilon_{bc}^{\lambda_1'}(\mathbf{k}'-\mathbf{p}') \varepsilon_{lm}^{\lambda_2'}(\mathbf{p}') p'^b p'^c \right)$
$j = 7$	$\delta^{\lambda\lambda'} \left(\varepsilon^{\lambda,lm}(\mathbf{k}) \varepsilon_{mc}^{\lambda_1}(\mathbf{k}-\mathbf{p}) \varepsilon_{lb}^{\lambda_2}(\mathbf{p}) (k-p)^b p^c \right) \left(\varepsilon^{\lambda',lm}(\mathbf{k}') \varepsilon^{\lambda_1',bc}(\mathbf{k}'-\mathbf{p}') \varepsilon_{bc}^{\lambda_2'}(\mathbf{p}') p'_l p'_m \right)$
$k^4 \mathbb{P}^{ij}$	$i = 6$
$j = 6$	$\delta^{\lambda\lambda'} \left(\varepsilon^{\lambda,lm}(\mathbf{k}) \varepsilon_{bc}^{\lambda_1}(\mathbf{k}-\mathbf{p}) \varepsilon_{lm}^{\lambda_2}(\mathbf{p}) p^b p^c \right) \left(\varepsilon^{\lambda',lm}(\mathbf{k}') \varepsilon_{bc}^{\lambda_1'}(\mathbf{k}'-\mathbf{p}') \varepsilon_{lm}^{\lambda_2'}(\mathbf{p}') p'^b p'^c \right)$
$j = 7$	$\delta^{\lambda\lambda'} \left(\varepsilon^{\lambda,lm}(\mathbf{k}) \varepsilon_{bc}^{\lambda_1}(\mathbf{k}-\mathbf{p}) \varepsilon_{lm}^{\lambda_2}(\mathbf{p}) p^b p^c \right) \left(\varepsilon^{\lambda',lm}(\mathbf{k}') \varepsilon^{\lambda_1',bc}(\mathbf{k}'-\mathbf{p}') \varepsilon_{bc}^{\lambda_2'}(\mathbf{p}') p'_l p'_m \right)$
$k^4 \mathbb{P}^{ij}$	$i = 7$
$j = 7$	$\delta^{\lambda\lambda'} \left(\varepsilon^{\lambda,lm}(\mathbf{k}) \varepsilon^{\lambda_1,bc}(\mathbf{k}-\mathbf{p}) \varepsilon_{bc}^{\lambda_2}(\mathbf{p}) p_l p_m \right) \left(\varepsilon^{\lambda',lm}(\mathbf{k}') \varepsilon^{\lambda_1',bc}(\mathbf{k}'-\mathbf{p}') \varepsilon_{bc}^{\lambda_2'}(\mathbf{p}') p'_l p'_m \right)$

Table 1: The explicit expressions of momentum polynomials $\mathbb{P}^{ij}(\mathbf{k}, \mathbf{p}, \mathbf{k}', \mathbf{p}')$.

In this paper, we consider the primordial power spectra $\mathcal{P}_\zeta^{(1)}(k)$ and $\mathcal{P}_h^{(1)}(k)$ with log-normal

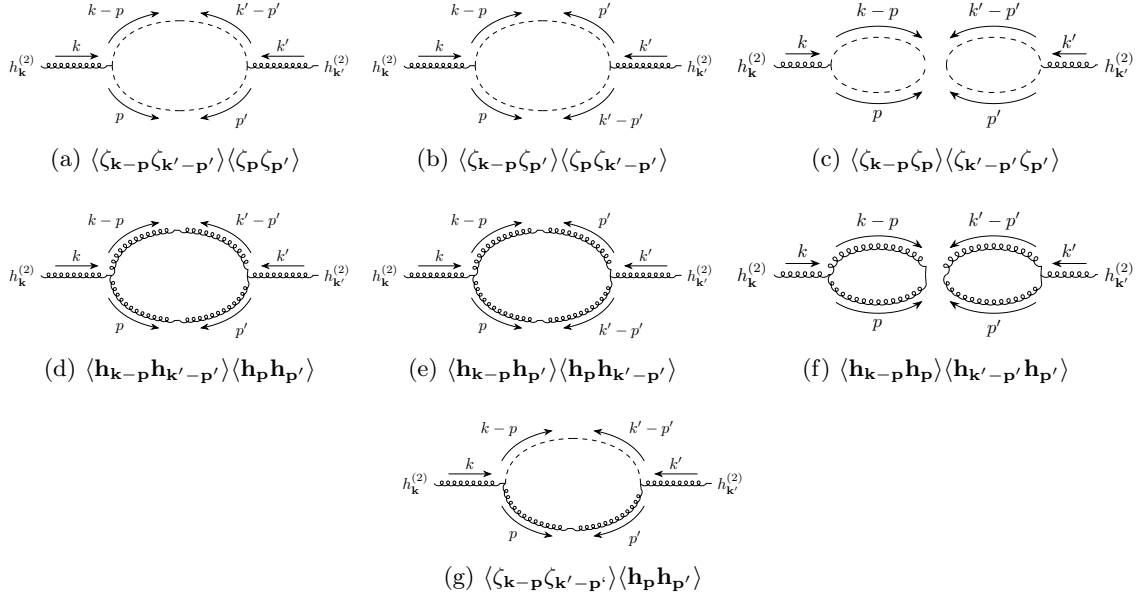


Figure 1: The diagrams correspond to the Wick's expansions of four-point correlation functions of primordial perturbations. The dashed and spring-like lines in the figure represent scalar and tensor perturbations, respectively.

peaks at the same location k_* on small scales

$$\begin{aligned} \mathcal{P}_\zeta^{(1)}(k) &= \frac{A_\zeta}{\sqrt{2\pi\sigma_*^2}} \exp\left(-\frac{\ln^2(k/k_*)}{2\sigma_*^2}\right), \\ \mathcal{P}_h^{(1)}(k) &= \frac{A_h}{\sqrt{2\pi\sigma_*^2}} \exp\left(-\frac{\ln^2(k/k_*)}{2\sigma_*^2}\right), \end{aligned} \quad (3.9)$$

where k_* is the wave number at which the power spectrum has a log-normal peak. A_ζ and A_h are amplitudes of primordial curvature and tensor power spectra respectively. σ_* is the parameter describing the widths of primordial power spectra. In the limit of $\sigma_* \rightarrow 0$, $\mathcal{P}_\zeta^{(1)}(k)$ and $\mathcal{P}_h^{(1)}(k)$ reduce to the monochromatic power spectra. Taking into account the thermal history of the universe, the current total energy density spectrum $\bar{\Omega}_{\text{GW},0}^{\text{tot}}(k)$ is given by

$$\bar{\Omega}_{\text{GW},0}^{\text{tot}}(k) = \Omega_{\text{rad},0} \left(\frac{g_{*,\rho,e}}{g_{*,\rho,0}} \right) \left(\frac{g_{*,s,0}}{g_{*,s,e}} \right)^{4/3} \bar{\Omega}_{\text{GW}}^{\text{tot}}(\eta, k), \quad (3.10)$$

where $\Omega_{\text{rad},0} (= 4.2 \times 10^{-5} h^{-2})$ is the energy density fraction of radiations today. Fig. 2 presents a comparison between the energy density spectrum of second-order SIGWs and the energy density spectra described in Eq. (3.1).

4 Detection of TSIGWs

In this section, we analyze how cosmological observations across various scales constrain second-order TSIGWs. Specifically, we consider the SGWBs dominated by PGWs+TSIGWs. By incorporating the energy density spectrum of TSIGWs studied in Sec. 3, we perform a Bayesian analysis to current PTA observations to determine or limit the parameter space of the primordial power spectrum. Since the tensor-scalar and tensor-tensor source terms significantly influence the total energy density spectrum of GWs at high frequencies, we thoroughly investigate the impact of small-scale PGWs+TSIGWs on SNR of LISA. Furthermore, PGWs and TSIGWs can

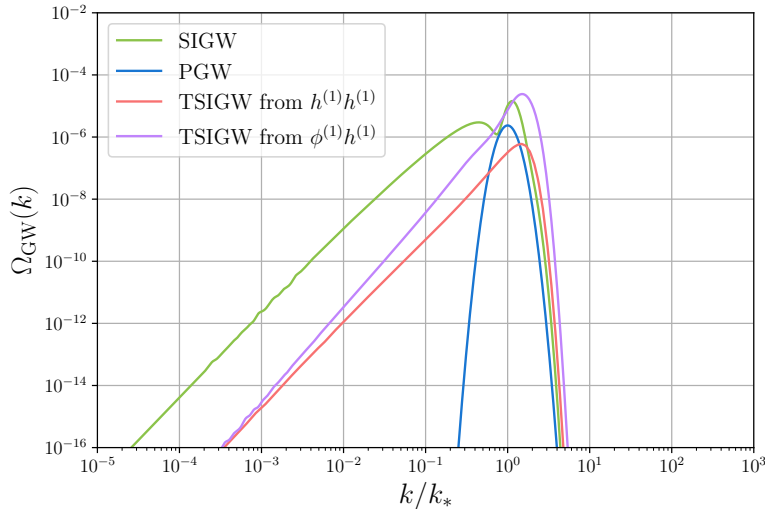


Figure 2: The energy spectra contributions from SIGWs, PGWs, tensor-tensor sources, and tensor-scalar sources are depicted by the green, blue, red, and purple lines, respectively. Parameters are set to $A_\zeta = A_h = 1$ and $\sigma_* = 0.2$.

serve as an extra radiation component, influencing the CMB and BAO observations. Based on current CMB and BAO observational data, we can constrain the parameter space of the small-scale primordial power spectrum.

4.1 PTA observations

To constrain the parameter space of primordial power spectra from PTA observations, we employ the kernel density estimator (KDE) representations of the free spectra to construct the likelihood function [82–84]

$$\ln \mathcal{L}(d|\theta) = \sum_{i=1}^{N_f} p(\Phi_i, \theta). \quad (4.1)$$

Here $p(\Phi_i, \theta)$ represents the probability of Φ_i given the parameter θ , and $\Phi_i = \Phi(f_i)$ denotes the time delay

$$\Phi(f) = \sqrt{\frac{H_0^2 \Omega_{\text{GW}}(f)}{8\pi^2 f^5 T_{\text{obs}}}}, \quad (4.2)$$

where $H_0 = h \times 100 \text{ km/s/Mpc}$ is the present-day value of the Hubble constant. We directly use the KDEs representation of the first 14 frequency HD-correlated free spectrum in NANOGrav 15-year dataset [85]. Bayesian analysis is performed by BILBY [86] with its built-in DYNESTY nested sampler [87, 88]. The spectrum of SMBHBs is modeled as power law [40, 82]

$$\Omega_{\text{GW}}(f) = \frac{2\pi^2 A_{\text{BHB}}^2}{3H_0^2 h^2} \left(\frac{f}{\text{year}^{-1}}\right)^{5-\gamma_{\text{BHB}}} \text{year}^{-2}. \quad (4.3)$$

The prior distribution for $(\log_{10} A_{\text{BHB}}, \gamma_{\text{BHB}})$ follows a multivariate normal distribution [40], whose mean and covariance matrix are given by

$$\boldsymbol{\mu}_{\text{BHB}} = \begin{pmatrix} -15.6 \\ 4.7 \end{pmatrix}, \boldsymbol{\sigma}_{\text{BHB}} = 0.1 \times \begin{pmatrix} 2.8 & -0.026 \\ -0.026 & 2.8 \end{pmatrix}. \quad (4.4)$$

We employ the Bayes factor to compare different models. The Bayes factor is defined as $B_{i,j} = \frac{Z_i}{Z_j}$, where Z_i represents the evidence of model H_i . Fig. 3 illustrates Bayes factors for comparisons

between various models and the SMBHB model. As shown in Fig. 3, the Bayes factor corresponding to PGWs+TSIGWs+SMBHB is the largest. Therefore, PGWs+TSIGWs are more likely to dominate the SGWBs observed by current PTA experiments than SMBHB.

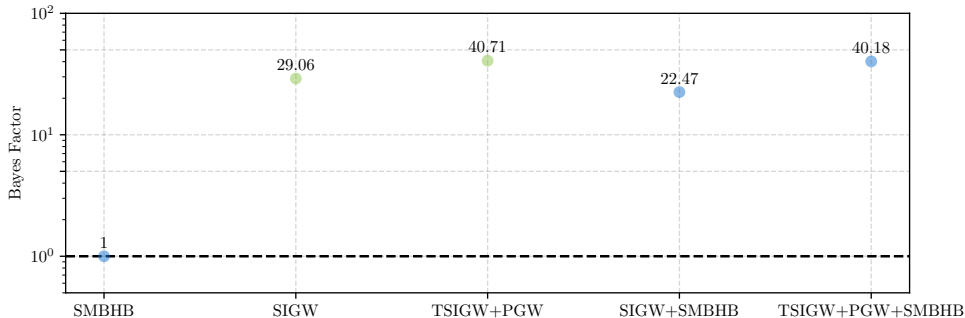


Figure 3: The Bayes factors between different models. The vertical axis represents the Bayes factor of different models relative to SMBHB, and the horizontal axis represents the different models. The green dots are for models without SMBHB and the blue dots are for models in combination with the SMBHB signal.

The posterior distributions of different models in Fig. 3 are presented in Fig. 4a and Fig. 4b, where prior distributions for $\log_{10}(f_*/\text{Hz})$, $\log_{10}(A_\zeta)$, $\log_{10}(A_h)$, and σ_* are uniform over the intervals $[-10, 3]$, $[-3, 1]$, $[-3, 1]$, and $[0.1, 1.5]$, respectively. More precisely, in Fig. 4a, we have ignored small-scale PGWs, focusing on scenarios where SIGWs are the primary contributors to current PTA observations and where both second-order SIGWs and SMBHB contribute to PTA observations. In Fig. 4b, we examine the scenarios where PGWs+TSIGWs dominate current PTA observations and where PGWs+TSIGWs and SMBHB jointly dominate PTA observations. Comparing the posterior distributions in Fig. 4a and Fig. 4b reveals that, when considering large-amplitude PGWs on small scales, the median value of A_ζ derived from current PTA observations is significantly reduced. Furthermore, since the total energy density spectrum of TSIGWs is composed of the four energy density spectra shown in Fig. 2, this leads to a degeneracy between the amplitudes of the primordial power spectra A_ζ and A_h . It should be noted that the degeneracy between parameters A_ζ and A_h only exists in the log-normal primordial power spectrum with large σ_* . For a monochromatic primordial power spectrum, the large-amplitude primordial tensor perturbations on small scales only affect the total energy density spectrum of GWs in the high-frequency region and do not affect the energy density spectrum in the low-frequency region [33]. In this scenario, the degeneracy between parameters A_ζ and A_h is not significant. Fig. 5 illustrates the total energy density spectra and compare the results with those of second-order SIGWs. Similar to the second-order SIGWs, the PGWs+TSIGWs in the case of a log-normal primordial power spectrum also fit well with current PTA observational data.

4.2 Signal-to-noise ratio of LISA

In the previous subsections, we investigated the effects of PGWs+TSIGWs on current PTA observations. As discussed in Sec. 3, large-amplitude PGWs on small scales significantly affect the total energy density spectrum of induced GWs in the high-frequency region. Therefore, in this subsection, we discuss the impact of PGWs+TSIGWs on the SNR of LISA to quantitatively assess their effect on the total energy density spectrum in the high-frequency region. The SNR of LISA can be expressed as [89, 90]

$$\rho = \sqrt{T} \left[\int df \left(\frac{\bar{\Omega}_{\text{GW},0}(f)}{\Omega_n(f)} \right)^2 \right]^{1/2}, \quad (4.5)$$

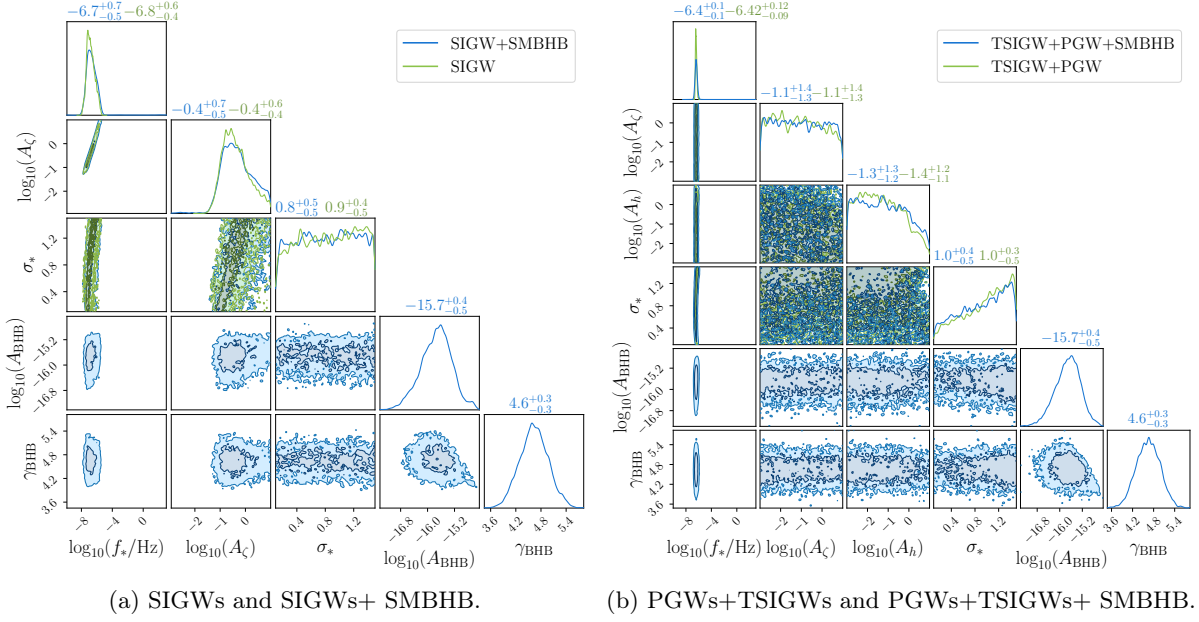


Figure 4: The corner plot of the posterior distributions. The contours in the off-diagonal panels denote the 68% and 95% credible intervals of the 2D posteriors. The numbers above the figures represent the median values and 1- σ ranges of the parameters. **Left panel:** The blue and green solid curves correspond to the SIGW energy spectrum with or without SMBHB. **Right panel:** The blue and green solid curves correspond to the PGWs+TSIGW energy spectrum with or without SMBHB.

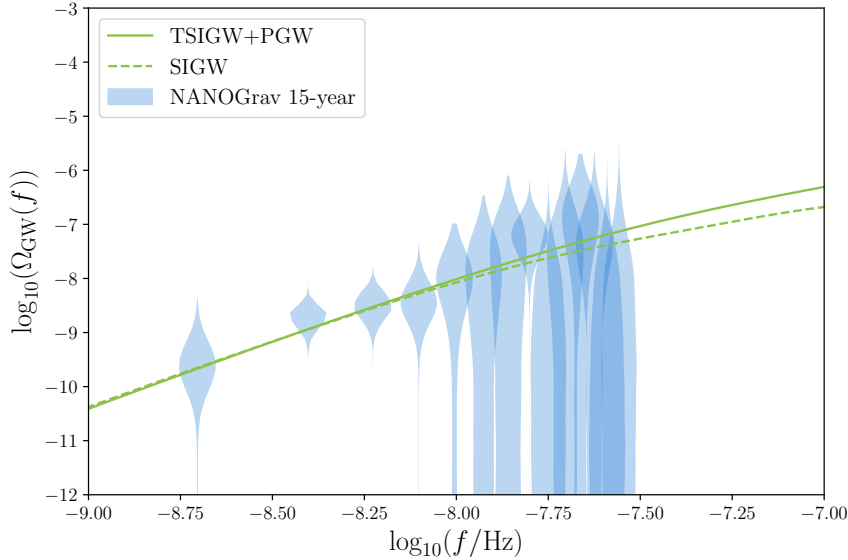


Figure 5: The spectra energy density of PGWs+TSIGWs and SIGWs. The energy density spectra derived from the free spectrum of the NANOGrav 15-year are shown with blue. The green curves represent the energy density spectra of GWs with different line styles labeled in the figure. Specifically, the parameters for the green solid line are: $\log_{10}(A_c) = -1.12$, $\log_{10}(A_h) = -1.39$, $\log_{10}(f_*/\text{Hz}) = -6.42$, and $\sigma_* = 1.04$; and for the green dashed line, the parameters are: $\log_{10}(A_c) = -0.44$, $\log_{10}(f_*/\text{Hz}) = -6.85$, and $\sigma_* = 0.85$. These parameters are selected based on the median values of the posterior distributions.

where T is the observation time and we set $T = 4$ years here. $\Omega_n(f) = 2\pi^2 f^3 S_n / 3H_0^2$, where H_0 is the Hubble constant, S_n is the strain noise power spectral density [90]. Fig. 6 shows the SNR curves for LISA experiments. ρ_{SIGW} and $\rho_{\text{TSIGW+PGW}}$ represent the SNR for the second-order SIGWs and PGWs+TSIGWs, respectively. Fig. 6 demonstrates that the existence of PGWs substantially increases SNR of LISA in the high-frequency range. Moreover, Fig. 7a and Fig. 7b illustrate the two-dimensional distribution of the SNR of LISA across various primordial power spectrum parameters. The red areas in Fig. 7a and Fig. 7b correspond to the 68% credible intervals of the 2D posterior distribution, determined when TSIGWs dominate PTA observations. As depicted in Fig. 6, with the rise in the amplitudes A_ζ and A_h of the primordial power spectra,

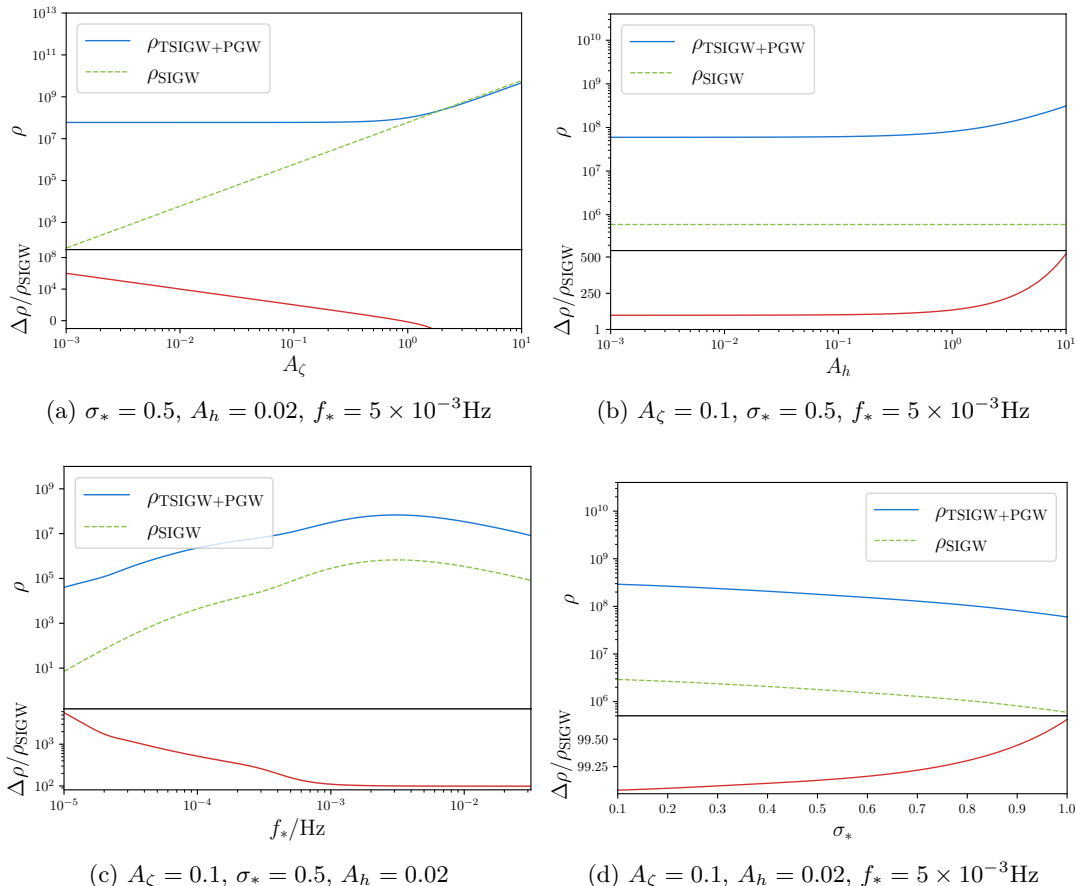


Figure 6: The SNR of LISA as a function of the parameters in primordial power spectra for both the SIGWs and PGWs+TSIGWs. The curves below show the improvement of SNR after considering the effects of PGWs. $\Delta\rho = |\rho_{\text{TSIGW+PGW}} - \rho_{\text{SIGW}}|$.

the energy density spectrum of PGWs+TSIGWs will increase, leading to a gradual increase in the SNR of LISA. In Fig. 7b, the parameter f_* indicates the position of the peak of the log-normal primordial power spectrum in Eq. (3.9), which also determines the frequency band of the energy density spectrum of PGWs+TSIGWs. As the parameter f_* increases, the energy density spectrum of PGWs+TSIGWs will gradually shift entirely into the detection band of LISA, resulting in an increase in SNR of LISA.

4.3 Constraints from CMB and BAO

Following the discussion in the previous subsection, TSIGWs, which are a significant source of the SGWBs, affect PTA observations. Additionally, they can serve as an extra radiation component, thereby influencing the cosmological observations on large scales [71, 98]. More precisely, the

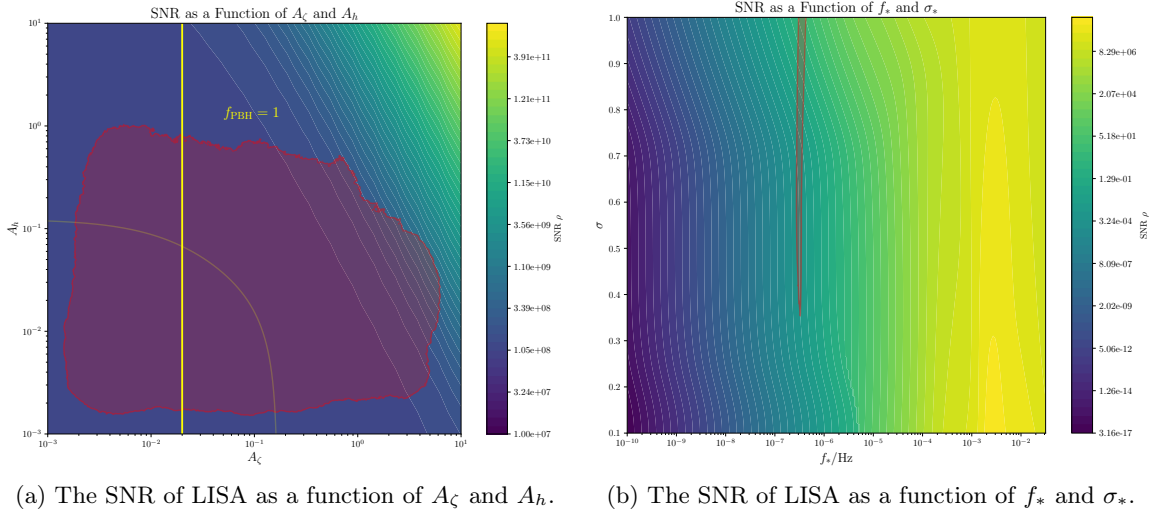


Figure 7: **Left panel:** The SNR of LISA as a function of A_ζ and A_h . The heatmap shows the SNR for fixed values of $f_* = 5 \times 10^{-3}$ Hz and $\sigma_* = 0.5$. The red shade represents the 68% credible intervals of the 2D posterior distribution in Fig. 4b, obtained through the KDE method implemented in the software ChainConsumer [91, 92]. The yellow shade shows the constraints from CMB and BAO when $\sigma_* = 0.5$, which are independent of f_* . The yellow line represents the curve for $f_* \approx 10^{-8}$ Hz, $\sigma_* = 0.5$, $f_{\text{PBH}} = 1$, indicating that all of dark matter is composed of primordial black holes (PBHs) [93–97]. **Right panel:** the SNR of LISA as a function of f_* and σ_* . The heatmap shows the SNR for fixed values of $A_\zeta = 0.1$ and $A_h = 0.02$. The red shade represents the 68% credible intervals of the 2D posterior distribution in Fig. 4b.

total energy density of GWs satisfies [98–101]

$$h^2 \rho_{\text{GW}} = \int_{f_{\text{min}}}^{\infty} h^2 \Omega_{\text{GW},0}(k) d(\ln k) < 2.9 \times 10^{-7} \quad (4.6)$$

at 95% confidence level for CMB+BAO data [71]. As shown in the yellow shade in Fig. 7a, we present the current CMB+BAO observational data constraints on the parameter space of the amplitude of primordial power spectra. As discussed in Sec. 4.2, the red shaded area in Fig. 7a represents the parameter space for the amplitude of the primordial power spectrum as determined by PTA observations. The overlap between the red and yellow shaded regions in Fig. 7a indicates the constraints on the parameter space for the amplitude of the primordial power spectrum provided by current CMB+BAO+PTA observations. Furthermore, the constraints on the abundance of primordial black holes (PBHs) dictate that the parameter A_ζ should not be greater than the yellow line shown in Fig. 7a. In summary, the main results regarding the amplitude of the primordial power spectrum in this paper are as follows:

The overlapping area of the red and yellow shaded regions to the left of the yellow line in Fig. 7a indicates the parameter space for the amplitude of the primordial power spectrum permitted by current cosmological observations (CMB+BAO+PTA+PBHs).

The results show that if PGWs+TSIGWs dominates the current PTA observations, the amplitude of power spectrum of primordial curvature perturbation is about 10^{-2} . In this study, we only consider the Gaussian primordial perturbations. In the case of local-type primordial non-Gaussianity, if we only consider second-order SIGWs or TSIGWs, the effects of local-type primordial non-Gaussianity do not significantly affect the total energy density spectrum of GWs.

However, when the primordial perturbations on small scales are substantial, the contributions from third-order and higher-order induced GWs become significant. As indicated in Ref. [30], the cross-correlation function $\langle h_{\mathbf{k}}^{\lambda,(3)}(\eta)h_{\mathbf{k}'}^{\lambda',(2)}(\eta) \rangle$ between second-order SIGWs and third-order SIGWs is proportional to the five-point correlation function of the primordial curvature perturbation: $\langle \zeta_{\mathbf{k}-\mathbf{p}}\zeta_{\mathbf{p}-\mathbf{q}}\zeta_{\mathbf{q}}\zeta_{\mathbf{k}'-\mathbf{p}'}\zeta_{\mathbf{p}'} \rangle$. Consequently, $\langle h_{\mathbf{k}}^{\lambda,(3)}(\eta)h_{\mathbf{k}'}^{\lambda',(2)}(\eta) \rangle$ contributes to the energy density spectrum of gravitational waves only in the presence of primordial non-Gaussianity, with its contribution being proportional to $f_{\text{NL}}A_{\zeta}^3 + (f_{\text{NL}})^3A_{\zeta}^4 + (f_{\text{NL}})^5A_{\zeta}^5$. When the non-Gaussian parameter f_{NL} is negative, the cross-correlation function $\langle h_{\mathbf{k}}^{\lambda,(3)}(\eta)h_{\mathbf{k}'}^{\lambda',(2)}(\eta) \rangle$ will notably suppress the total energy density spectrum of induced GWs. Therefore, the conclusion here may be affected by various physical processes during the evolution of the universe, such as the impact of primordial non-Gaussianity [31, 60, 102], varying sound speed [59, 103], interactions between induced gravitational waves and matter [20–22, 104–106], and higher-order effects [29, 30]. Moreover, as depicted in Fig. 7b by the red shaded regions, the SNR of LISA is quite minimal within the parameter space identified by PTA observations. Therefore, the conclusions on TSIGWs observations in this paper are as follows:

If the TSIGWs+PGWs dominates the SGWBs observed in the current PTA frequency band, its impact on the SGWBs observations in the future LISA frequency band is negligible.

The conclusions above provide a method for identifying different sources of the SGWBs, namely by observing SGWBs on different scales and combining other types of observational constraints (such as PBHs, CMB, BAO etc.) to jointly constrain or determine the source of the SGWBs. This method is applicable not only to TSIGWs but also to other types of SGWBs generated in the early universe [107]. It should be noted that these results depend on the specific form of the primordial power spectrum, which may lead to different conclusions for different forms. For other forms of the primordial power spectra, we need to use the model-independent results given in Eq. (3.5)–Eq. (3.7) to recalculate the energy density spectrum of TSIGWs.

5 Conclusion and discussion

Primordial curvature and tensor perturbations may exhibit significant amplitudes at small scales, potentially inducing higher-order GWs with observable effects. In this paper, we investigated second-order TSIGWs during the RD era. The source terms of second-order TSIGWs are divided into three types: scalar-scalar, tensor-scalar, and tensor-tensor sources. When ignoring large-amplitude primordial tensor perturbations at small scales, our results for second-order TSIGWs align with the results of second-order SIGWs. We provided explicit expressions for the energy density spectrum of second-order TSIGWs. Considering a log-normal primordial power spectrum, we utilized current CMB+BAO+PTA+PBHs observational data to constrain the parameter space of the small-scale primordial power spectrum. Furthermore, we analyzed the impact of different primordial power spectrum parameters on the SNR of LISA in the high-frequency region. The specific constraints on the parameter space of primordial curvature and tensor perturbations from current observations are shown in the overlapping area of the red and yellow shaded regions to the left of the yellow line in Fig. 7a. The presence of large-amplitude primordial tensor perturbations on small scales can prevent the overproduction of PBHs [108].

The results we presented in Eq. (3.5)–Eq. (3.7) are applicable to any form of primordial curvature perturbation and primordial tensor perturbation power spectra. Given specific primordial power spectra, we can calculate the corresponding energy density spectrum of second-order TSIGWs. Notably, when the peaks of the primordial curvature and tensor perturbation power spectra occur at different scales, the second-order GWs induced by tensor-scalar sources can be very large. This potential "divergence" issue in the energy density spectrum of second-order

TSIGWs has been studied in Refs. [35, 37]. Ref. [35] provides a phenomenological method to mitigate such divergence by inserting a correction factor $f(u) = \frac{u^4}{d^4+u^4}$ into Eq. (3.6) to "dilute" the potential divergence effect. Understanding the potential "divergence" issue within tensor-scalar sources remains an unresolved question and may be further refined in future research.

In current studies of second-order TSIGWs, the chosen primordial power spectra are typically parameterized log-normal primordial power spectra. For specific primordial power spectra provided by particular inflation models, we can use Eq. (3.5)–Eq. (3.7) to calculate the energy density spectrum of second-order TSIGWs and use the cosmological observations at different scales given in Sec. 4 to constrain the parameter space of these inflation models. Furthermore, as illustrated in Fig. 1, we focus primarily on the one-loop contributions from the two-point correlation function $\langle h_{\mathbf{k}}^{\lambda,(2)} h_{\mathbf{k}'}^{\lambda',(2)} \rangle$. The one-loop contributions from the two-point correlation function $\langle h_{\mathbf{k}}^{\lambda,(3)} h_{\mathbf{k}'}^{\lambda',(1)} \rangle$, as considered in Ref. [109], and the two-loop contributions similar to the SIGWs studies [29], have not been systematically investigated. The comprehensive one-loop calculations for TSIGWs, along with the corresponding two-loop calculations, may be further developed in future research.

Acknowledgments

We thank Dr. Y.H. Yu for the useful discussions. The work is supported in part by the National Natural Science Foundation of China (NSFC) grants No.12475075, No. 11935009, No. 12375052, and No. 12447127.

References

- [1] D. Baumann, *Cosmology*, Cambridge University Press (7, 2022), [10.1017/9781108937092](https://doi.org/10.1017/9781108937092).
- [2] K.A. Malik and D. Wands, *Cosmological perturbations*, *Phys. Rept.* **475** (2009) 1 [[0809.4944](https://arxiv.org/abs/0809.4944)].
- [3] Y. Wang, *Inflation, Cosmic Perturbations and Non-Gaussianities*, *Commun. Theor. Phys.* **62** (2014) 109 [[1303.1523](https://arxiv.org/abs/1303.1523)].
- [4] D. Baumann, *Inflation*, in *Theoretical Advanced Study Institute in Elementary Particle Physics: Physics of the Large and the Small*, pp. 523–686, 2011, DOI [[0907.5424](https://arxiv.org/abs/0907.5424)].
- [5] T.H.-C. Lu, K. Ananda, C. Clarkson and R. Maartens, *The cosmological background of vector modes*, *JCAP* **02** (2009) 023 [[0812.1349](https://arxiv.org/abs/0812.1349)].
- [6] PLANCK collaboration, *Planck 2018 results. VI. Cosmological parameters*, *Astron. Astrophys.* **641** (2020) A6 [[1807.06209](https://arxiv.org/abs/1807.06209)].
- [7] PLANCK collaboration, *Planck 2015 results. XIII. Cosmological parameters*, *Astron. Astrophys.* **594** (2016) A13 [[1502.01589](https://arxiv.org/abs/1502.01589)].
- [8] PLANCK collaboration, *Planck 2015 results. XX. Constraints on inflation*, *Astron. Astrophys.* **594** (2016) A20 [[1502.02114](https://arxiv.org/abs/1502.02114)].
- [9] PLANCK collaboration, *Planck 2018 results. V. CMB power spectra and likelihoods*, *Astron. Astrophys.* **641** (2020) A5 [[1907.12875](https://arxiv.org/abs/1907.12875)].
- [10] E. Abdalla et al., *Cosmology intertwined: A review of the particle physics, astrophysics, and cosmology associated with the cosmological tensions and anomalies*, *JHEAp* **34** (2022) 49 [[2203.06142](https://arxiv.org/abs/2203.06142)].
- [11] L. Perivolaropoulos and F. Skara, *Challenges for Λ CDM: An update*, *New Astron. Rev.* **95** (2022) 101659 [[2105.05208](https://arxiv.org/abs/2105.05208)].
- [12] PLANCK collaboration, *Planck 2018 results. X. Constraints on inflation*, *Astron. Astrophys.* **641** (2020) A10 [[1807.06211](https://arxiv.org/abs/1807.06211)].
- [13] T. Bringmann, P. Scott and Y. Akrami, *Improved constraints on the primordial power spectrum at small scales from ultracompact minihalos*, *Phys. Rev. D* **85** (2012) 125027 [[1110.2484](https://arxiv.org/abs/1110.2484)].

- [14] B. Carr, K. Kohri, Y. Sendouda and J. Yokoyama, *Constraints on primordial black holes*, *Rept. Prog. Phys.* **84** (2021) 116902 [[2002.12778](#)].
- [15] G. Domènech, *Scalar Induced Gravitational Waves Review*, *Universe* **7** (2021) 398 [[2109.01398](#)].
- [16] S. Matarrese, S. Mollerach and M. Bruni, *Second order perturbations of the Einstein-de Sitter universe*, *Phys. Rev. D* **58** (1998) 043504 [[astro-ph/9707278](#)].
- [17] S. Mollerach, D. Harari and S. Matarrese, *CMB polarization from secondary vector and tensor modes*, *Phys. Rev. D* **69** (2004) 063002 [[astro-ph/0310711](#)].
- [18] K.N. Ananda, C. Clarkson and D. Wands, *The Cosmological gravitational wave background from primordial density perturbations*, *Phys. Rev. D* **75** (2007) 123518 [[gr-qc/0612013](#)].
- [19] D. Baumann, P.J. Steinhardt, K. Takahashi and K. Ichiki, *Gravitational Wave Spectrum Induced by Primordial Scalar Perturbations*, *Phys. Rev. D* **76** (2007) 084019 [[hep-th/0703290](#)].
- [20] X. Zhang, J.-Z. Zhou and Z. Chang, *Impact of the free-streaming neutrinos to the second order induced gravitational waves*, *Eur. Phys. J. C* **82** (2022) 781 [[2208.12948](#)].
- [21] A. Mangilli, N. Bartolo, S. Matarrese and A. Riotto, *The impact of cosmic neutrinos on the gravitational-wave background*, *Phys. Rev. D* **78** (2008) 083517 [[0805.3234](#)].
- [22] S. Saga, K. Ichiki and N. Sugiyama, *Impact of anisotropic stress of free-streaming particles on gravitational waves induced by cosmological density perturbations*, *Phys. Rev. D* **91** (2015) 024030 [[1412.1081](#)].
- [23] T. Papanikolaou, C. Tzerefos, S. Basilakos and E.N. Saridakis, *Scalar induced gravitational waves from primordial black hole Poisson fluctuations in $f(R)$ gravity*, *JCAP* **10** (2022) 013 [[2112.15059](#)].
- [24] J.-P. Li, S. Wang, Z.-C. Zhao and K. Kohri, *Primordial Non-Gaussianity and Anisotropies in Gravitational Waves induced by Scalar Perturbations*, [2305.19950](#).
- [25] C. Chen and A. Ota, *Induced gravitational waves from statistically anisotropic scalar perturbations*, *Phys. Rev. D* **106** (2022) 063507 [[2205.07810](#)].
- [26] J.-Z. Zhou, X. Zhang, Q.-H. Zhu and Z. Chang, *The third order scalar induced gravitational waves*, *JCAP* **05** (2022) 013 [[2106.01641](#)].
- [27] Z. Chang, Y.-T. Kuang, X. Zhang and J.-Z. Zhou, *Primordial black holes and third order scalar induced gravitational waves**, *Chin. Phys. C* **47** (2023) 055104 [[2209.12404](#)].
- [28] Z. Chang, X. Zhang and J.-Z. Zhou, *The cosmological vector modes from a monochromatic primordial power spectrum*, *JCAP* **10** (2022) 084 [[2207.01231](#)].
- [29] Z. Chang, Y.-T. Kuang, D. Wu and J.-Z. Zhou, *Probing scalar induced gravitational waves with PTA and LISA: the importance of third order correction*, *JCAP* **2024** (2024) 044 [[2312.14409](#)].
- [30] Z. Chang, Y.-T. Kuang, D. Wu, J.-Z. Zhou and Q.-H. Zhu, *New constraints on primordial non-Gaussianity from missing two-loop contributions of scalar induced gravitational waves*, *Phys. Rev. D* **109** (2024) L041303 [[2311.05102](#)].
- [31] A.J. Iovino, S. Matarrese, G. Perna, A. Ricciardone and A. Riotto, *How Well Do We Know the Scalar-Induced Gravitational Waves?*, [2412.06764](#).
- [32] B.-Q. Lu, *Scalar-induced gravitational wave from domain wall perturbation*, [2412.07677](#).
- [33] Z. Chang, X. Zhang and J.-Z. Zhou, *Gravitational waves from primordial scalar and tensor perturbations*, *Phys. Rev. D* **107** (2023) 063510 [[2209.07693](#)].
- [34] Y.-H. Yu and S. Wang, *Primordial Gravitational Waves Assisted by Cosmological Scalar Perturbations*, [2303.03897](#).
- [35] P. Bari, N. Bartolo, G. Domènech and S. Matarrese, *Gravitational waves induced by scalar-tensor mixing*, [2307.05404](#).
- [36] J.-O. Gong, *Analytic Integral Solutions for Induced Gravitational Waves*, *Astrophys. J.* **925** (2022) 102 [[1909.12708](#)].
- [37] R. Picard and K.A. Malik, *Induced gravitational waves: the effect of first order tensor perturbations*, *JCAP* **10** (2024) 010 [[2311.14513](#)].

- [38] K. Inomata and T. Nakama, *Gravitational waves induced by scalar perturbations as probes of the small-scale primordial spectrum*, *Phys. Rev. D* **99** (2019) 043511 [[1812.00674](#)].
- [39] NANOGrav collaboration, *The NANOGrav 15 yr Data Set: Evidence for a Gravitational-wave Background*, *Astrophys. J. Lett.* **951** (2023) L8 [[2306.16213](#)].
- [40] NANOGrav collaboration, *The NANOGrav 15 yr Data Set: Search for Signals from New Physics*, *Astrophys. J. Lett.* **951** (2023) L11 [[2306.16219](#)].
- [41] EPTA collaboration, *The second data release from the European Pulsar Timing Array III. Search for gravitational wave signals*, [2306.16214](#).
- [42] D.J. Reardon et al., *Search for an Isotropic Gravitational-wave Background with the Parkes Pulsar Timing Array*, *Astrophys. J. Lett.* **951** (2023) L6 [[2306.16215](#)].
- [43] H. Xu et al., *Searching for the Nano-Hertz Stochastic Gravitational Wave Background with the Chinese Pulsar Timing Array Data Release I*, *Res. Astron. Astrophys.* **23** (2023) 075024 [[2306.16216](#)].
- [44] H. Middleton, A. Sesana, S. Chen, A. Vecchio, W. Del Pozzo and P.A. Rosado, *Massive black hole binary systems and the NANOGrav 12.5 yr results*, *Mon. Not. Roy. Astron. Soc.* **502** (2021) L99 [[2011.01246](#)].
- [45] NANOGrav collaboration, *Astrophysics Milestones for Pulsar Timing Array Gravitational-wave Detection*, *Astrophys. J. Lett.* **911** (2021) L34 [[2010.11950](#)].
- [46] K. Fujikura, S. Girmohanta, Y. Nakai and M. Suzuki, *NANOGrav Signal from a Dark Conformal Phase Transition*, [2306.17086](#).
- [47] A. Addazi, Y.-F. Cai, A. Marciano and L. Visinelli, *Have pulsar timing array methods detected a cosmological phase transition?*, [2306.17205](#).
- [48] S. Jiang, A. Yang, J. Ma and F.P. Huang, *Implication of nano-Hertz stochastic gravitational wave on dynamical dark matter through a first-order phase transition*, [2306.17827](#).
- [49] Y. Xiao, J.M. Yang and Y. Zhang, *Implications of Nano-Hertz Gravitational Waves on Electroweak Phase Transition in the Singlet Dark Matter Model*, [2307.01072](#).
- [50] Y.-M. Wu, Z.-C. Chen and Q.-G. Huang, *Cosmological Interpretation for the Stochastic Signal in Pulsar Timing Arrays*, [2307.03141](#).
- [51] S. He, L. Li, S. Wang and S.-J. Wang, *Constraints on holographic QCD phase transitions from PTA observations*, [2308.07257](#).
- [52] J. Ellis and M. Lewicki, *Cosmic String Interpretation of NANOGrav Pulsar Timing Data*, *Phys. Rev. Lett.* **126** (2021) 041304 [[2009.06555](#)].
- [53] J. Ellis, M. Lewicki, C. Lin and V. Vaskonen, *Cosmic Superstrings Revisited in Light of NANOGrav 15-Year Data*, [2306.17147](#).
- [54] G. Lazarides, R. Maji and Q. Shafi, *Superheavy quasi-stable strings and walls bounded by strings in the light of NANOGrav 15 year data*, [2306.17788](#).
- [55] M. Yamada and K. Yonekura, *Dark baryon from pure Yang-Mills theory and its GW signature from cosmic strings*, [2307.06586](#).
- [56] Z.-Y. Qiu and Z.-H. Yu, *Gravitational waves from cosmic strings associated with pseudo-Nambu-Goldstone dark matter**, *Chin. Phys. C* **47** (2023) 085104 [[2304.02506](#)].
- [57] V. Vaskonen and H. Veermäe, *Did NANOGrav see a signal from primordial black hole formation?*, *Phys. Rev. Lett.* **126** (2021) 051303 [[2009.07832](#)].
- [58] V. De Luca, G. Franciolini and A. Riotto, *NANOGrav Data Hints at Primordial Black Holes as Dark Matter*, *Phys. Rev. Lett.* **126** (2021) 041303 [[2009.08268](#)].
- [59] S. Balaji, G. Domènech and G. Franciolini, *Scalar-induced gravitational wave interpretation of PTA data: the role of scalar fluctuation propagation speed*, [2307.08552](#).
- [60] G. Franciolini, A. Iovino, Junior., V. Vaskonen and H. Veermäe, *The recent gravitational wave observation by pulsar timing arrays and primordial black holes: the importance of non-gaussianities*, [2306.17149](#).

- [61] Z.-Q. You, Z. Yi and Y. Wu, *Constraints on primordial curvature power spectrum with pulsar timing arrays*, [2307.04419](#).
- [62] Z.-C. Zhao, Q.-H. Zhu, S. Wang and X. Zhang, *Exploring the Equation of State of the Early Universe: Insights from BBN, CMB, and PTA Observations*, [2307.13574](#).
- [63] S. Wang, Z.-C. Zhao, J.-P. Li and Q.-H. Zhu, *Exploring the Implications of 2023 Pulsar Timing Array Datasets for Scalar-Induced Gravitational Waves and Primordial Black Holes*, [2307.00572](#).
- [64] Q.-H. Zhu, Z.-C. Zhao and S. Wang, *Joint implications of BBN, CMB, and PTA Datasets for Scalar-Induced Gravitational Waves of Second and Third orders*, [2307.03095](#).
- [65] H. Di and Y. Gong, *Primordial black holes and second order gravitational waves from ultra-slow-roll inflation*, *JCAP* **07** (2018) 007 [[1707.09578](#)].
- [66] L. Iacconi, M. Bacchi, L.F. Guimarães and F.T. Falciano, *Testing inflation on all scales: a case study with α -attractors*, [2412.02544](#).
- [67] C. Tzerefos, T. Papanikolaou, S. Basilakos, E.N. Saridakis and N.E. Mavromatos, *Gravitational wave signatures from reheating in Chern-Simons running-vacuum cosmology*, [2411.14223](#).
- [68] T. Kobayashi, M. Yamaguchi and J. Yokoyama, *G-inflation: Inflation with the most general second-order field equations*, *Int. J. Mod. Phys. Conf. Ser.* **10** (2012) 77.
- [69] Y.-F. Cai, C. Lin, B. Wang and S.-F. Yan, *Sound speed resonance of the stochastic gravitational wave background*, *Phys. Rev. Lett.* **126** (2021) 071303 [[2009.09833](#)].
- [70] M.A. Gorji and M. Sasaki, *Primordial-tensor-induced stochastic gravitational waves*, [2302.14080](#).
- [71] T.J. Clarke, E.J. Copeland and A. Moss, *Constraints on primordial gravitational waves from the Cosmic Microwave Background*, *JCAP* **10** (2020) 002 [[2004.11396](#)].
- [72] I. Ben-Dayan, B. Keating, D. Leon and I. Wolfson, *Constraints on scalar and tensor spectra from N_{eff}* , *JCAP* **06** (2019) 007 [[1903.11843](#)].
- [73] J. Cang, Y.-Z. Ma and Y. Gao, *Implications for Primordial Black Holes from Cosmological Constraints on Scalar-induced Gravitational Waves*, *Astrophys. J.* **949** (2023) 64 [[2210.03476](#)].
- [74] K. Kohri and T. Terada, *Semianalytic calculation of gravitational wave spectrum nonlinearly induced from primordial curvature perturbations*, *Phys. Rev. D* **97** (2018) 123532 [[1804.08577](#)].
- [75] C. Yuan and Q.-G. Huang, *A topic review on probing primordial black hole dark matter with scalar induced gravitational waves*, *iScience* **24** (2021) 102860 [[2103.04739](#)].
- [76] J.-Z. Zhou, Y.-T. Kuang, D. Wu, H. Lü and Z. Chang, *Induced gravitational waves for arbitrary higher orders: vertex rules and loop diagrams in cosmological perturbation theory*, [2408.14052](#).
- [77] H. Assadullahi and D. Wands, *Gravitational waves from an early matter era*, *Phys. Rev. D* **79** (2009) 083511 [[0901.0989](#)].
- [78] L. Alabidi, K. Kohri, M. Sasaki and Y. Sendouda, *Observable induced gravitational waves from an early matter phase*, *JCAP* **05** (2013) 033 [[1303.4519](#)].
- [79] G. Domènech, C. Lin and M. Sasaki, *Gravitational wave constraints on the primordial black hole dominated early universe*, *JCAP* **04** (2021) 062 [[2012.08151](#)].
- [80] T. Papanikolaou, V. Vennin and D. Langlois, *Gravitational waves from a universe filled with primordial black holes*, *JCAP* **03** (2021) 053 [[2010.11573](#)].
- [81] M. Maggiore, *Gravitational wave experiments and early universe cosmology*, *Phys. Rept.* **331** (2000) 283 [[gr-qc/9909001](#)].
- [82] A. Mitridate, D. Wright, R. von Eckardstein, T. Schröder, J. Nay, K. Olum et al., *PTArcade*, [2306.16377](#).
- [83] W.G. Lamb, S.R. Taylor and R. van Haasteren, *Rapid refitting techniques for Bayesian spectral characterization of the gravitational wave background using pulsar timing arrays*, *Phys. Rev. D* **108** (2023) 103019 [[2303.15442](#)].
- [84] C.J. Moore and A. Vecchio, *Ultra-low-frequency gravitational waves from cosmological and astrophysical processes*, *Nature Astron.* **5** (2021) 1268 [[2104.15130](#)].

- [85] T.N. Collaboration, *Kde representations of the gravitational wave background free spectra present in the nanograv 15-year dataset*, Dec., 2023. 10.5281/zenodo.10344086.
- [86] G. Ashton et al., *BILBY: A user-friendly Bayesian inference library for gravitational-wave astronomy*, *Astrophys. J. Suppl.* **241** (2019) 27 [1811.02042].
- [87] J.S. Speagle, *dynesty: a dynamic nested sampling package for estimating Bayesian posteriors and evidences*, *Mon. Not. Roy. Astron. Soc.* **493** (2020) 3132 [1904.02180].
- [88] S. Kopesov, J. Speagle, K. Barbary, G. Ashton, E. Bennett, J. Buchner et al., *joshspeagle/dynesty: v2.1.4*, June, 2024. 10.5281/zenodo.12537467.
- [89] X. Siemens, J. Ellis, F. Jenet and J.D. Romano, *The stochastic background: scaling laws and time to detection for pulsar timing arrays*, *Class. Quant. Grav.* **30** (2013) 224015 [1305.3196].
- [90] T. Robson, N.J. Cornish and C. Liu, *The construction and use of LISA sensitivity curves*, *Class. Quant. Grav.* **36** (2019) 105011 [1803.01944].
- [91] S. Hinton, *Chainconsumer*, *Journal of Open Source Software* **1** (2016) 45.
- [92] S. Hinton, S. Dupourqué, J. Zhang, S. wen DENG, and C. Badger, *Samreay/chainconsumer: Loosening dependencies*, Nov., 2024. 10.5281/zenodo.14172285.
- [93] B. Carr and F. Kuhnel, *Primordial Black Holes as Dark Matter: Recent Developments*, *Ann. Rev. Nucl. Part. Sci.* **70** (2020) 355 [2006.02838].
- [94] B. Carr, F. Kuhnel and M. Sandstad, *Primordial Black Holes as Dark Matter*, *Phys. Rev. D* **94** (2016) 083504 [1607.06077].
- [95] V. De Luca, G. Franciolini, A. Kehagias, M. Peloso, A. Riotto and C. Ünal, *The Ineludible non-Gaussianity of the Primordial Black Hole Abundance*, *JCAP* **07** (2019) 048 [1904.00970].
- [96] A.J. Iovino, G. Perna, A. Riotto and H. Veermäe, *Curbing PBHs with PTAs*, *JCAP* **10** (2024) 050 [2406.20089].
- [97] I. Musco, V. De Luca, G. Franciolini and A. Riotto, *Threshold for primordial black holes. II. A simple analytic prescription*, *Phys. Rev. D* **103** (2021) 063538 [2011.03014].
- [98] J.-Z. Zhou, Y.-T. Kuang, Z. Chang and H. Lü, *Constraints on primordial black holes from N_{eff} : scalar induced gravitational waves as an extra radiation component*, 2410.10111.
- [99] S. Wang, Z.-C. Zhao and Q.-H. Zhu, *Constraints on scalar-induced gravitational waves up to third order from a joint analysis of BBN, CMB, and PTA data*, *Phys. Rev. Res.* **6** (2024) 013207 [2307.03095].
- [100] D. Wright, J.T. Giblin and J. Hazboun, *CMB and energy conservation limits on nanohertz gravitational waves*, 2409.15572.
- [101] X.-B. Sui, J. Liu and R.-G. Cai, *Enhancement of small-scale induced gravitational waves from the soliton/oscillon domination*, 2412.08057.
- [102] R. Picard and M.W. Davies, *Effects of scalar non-Gaussianity on induced scalar-tensor gravitational waves*, 2410.17819.
- [103] J.-H. Jin, Z.-C. Chen, Z. Yi, Z.-Q. You, L. Liu and Y. Wu, *Confronting sound speed resonance with pulsar timing arrays*, *JCAP* **09** (2023) 016 [2307.08687].
- [104] Y.-H. Yu and S. Wang, *Silk damping in scalar-induced gravitational waves: a novel probe for new physics*, *Sci. China Phys. Mech. Astron.* **68** (2025) 210412 [2405.02960].
- [105] M. Loverde and Z.J. Weiner, *Probing neutrino interactions and dark radiation with gravitational waves*, *JCAP* **02** (2023) 064 [2208.11714].
- [106] X.-B. Sui, J. Liu, X.-Y. Yang and R.-G. Cai, *Detecting the dark sector through scalar-induced gravitational waves*, *Phys. Rev. D* **110** (2024) 103541 [2407.04220].
- [107] J. Ellis, M. Fairbairn, G. Franciolini, G. Hütsi, A. Iovino, M. Lewicki et al., *What is the source of the PTA GW signal?*, *Phys. Rev. D* **109** (2024) 023522 [2308.08546].
- [108] M.A. Gorji, M. Sasaki and T. Suyama, *Extra-tensor-induced origin for the PTA signal: No primordial black hole production*, *Phys. Lett. B* **846** (2023) 138214 [2307.13109].

- [109] C. Chen, A. Ota, H.-Y. Zhu and Y. Zhu, *Missing one-loop contributions in secondary gravitational waves*, *Phys. Rev. D* **107** (2023) 083518 [[2210.17176](#)].